frontiers | Frontiers in Environmental Science

TYPE Original Research
PUBLISHED 06 October 2022
DOI 10.3389/fenvs.2022.1009045

OPEN ACCESS

EDITED BY
yingxin ZhaO,
Tianjin University, China

REVIEWED BY
Dahu Ding,
Nanjing Agricultural University, China
Guangbo Che,
Jilin Normal University, China

*CORRESPONDENCE
Yingnan Yang,
yo.innan.fu@u.tsukuba.ac.jp

SPECIALTY SECTION
This article was submitted to Water and Wastewater Management, a section of the journal Frontiers in Environmental Science

RECEIVED 01 August 2022
ACCEPTED 21 September 2022
PUBLISHED 06 October 2022

CITATION
Liu N, Qi R, Sun X, Kawazoe N, Chen G and Yang Y (2022), Synthesis and characterization of 3D-zeolite–modified TiO_2-based photocatalyst with synergistic effect for elimination of organic pollutant in wastewater treatment.
Front. Environ. Sci. 10:1009045.
doi: 10.3389/fenvs.2022.1009045

Synthesis and characterization of 3D-zeolite–modified TiO_2-based photocatalyst with synergistic effect for elimination of organic pollutant in wastewater treatment

Na Liu[1,2], Ruilin Qi[2], Xiang Sun[2], Naoki Kawazoe[3], Guoping Chen[3] and Yingnan Yang[2]*

[1]Department of Biomedical Engineering, Chengde Medical University, Chengde, China, [2]Graduate School of Life and Environmental Science, University of Tsukuba, Tsukuba, Japan, [3]Research Center of Functional Materials, National Institute for Materials Science, Tsukuba, Japan

In this work, zeolite, a porous material with a 3D network structure, was introduced as the carrier to support $P/Ag/Ag_2O/Ag_3PO_4/TiO_2$ (PAgT) composite for synthesizing the 3D-zeolite–modified photocatalyst (Z-PAgT). In this combination, zeolite with strong adsorbability can pre-adsorb and condense organic compounds onto the catalyst surface, thereby helping to speed up the photocatalytic reaction. In the present study, to determine the optimum mass ratio of zeolite to photocatalyst, various samples containing different zeolite additions (0 wt%, 5 wt%, 10 wt%, and 25 wt%) were prepared using the hydrothermal method, respectively. The physical–chemical properties of the as-prepared samples were systematically characterized by different analytical techniques, including XRD, FTIR, SEM, BET, EDX, UV-Vis, and PL. The results revealed that the obtained Z-PAgT-5 sample possessed relatively higher crystallinity, smaller crystalline size, larger specific surface area, narrow band gap, and lower generated electron-hole recombination rate. The photocatalytic degradation of rhodamine B (Rh B) in aqueous suspension has been employed to evaluate the photocatalytic activity of the as-prepared photocatalysts with simulated solar light as an irradiation source. The results showed that Z-PAgT-5 performed the highest photodegradation efficiency, and its degradation rate constant (k_{app}) (0.188 min^{-1}) is much higher than that of Z-PAgT-0 (0.132 min^{-1}), Z-PAgT-10 (0.050 min^{-1}), Z-PAgT-25 (0.037 min^{-1}), and pure zeolite (0.003 min^{-1}). This super photocatalytic activity of Z-PAgT-5 toward Rh B degradation can be ascribed to the synergistic effect between the 3D-zeolite and PAgT photocatalyst, which made the hybrid zeolite-photocatalyst material possess good adsorption and photodegradation properties. In addition, repetitive experiments demonstrated that the improved Rh B degradation efficiency of Z-PAgT-5 was well maintained even after five recycling runs without any obvious decrease. Hence, the obtained results indicated that Z-PAgT-5 material can be used as a potential

photocatalyst for treating organic pollutants during wastewater environmental remediation.

KEYWORDS

3D-zeolite–modified PAgT photocatalyst, adsorption and photodegradation synergism, elimination of organic pollutant, solar light illumination, wastewater purification

Introduction

Nowadays, with the rapid development of modern industry and agriculture, the increased deterioration of water quality with the shortage of clean water resources is already posing a strict challenge to sustainable development for human beings (Takala, 2017). In the billions of tons of polluted wastewater, the toxic organic pollutant is the most prevalent, which is produced along with dye and pharmaceutical or paper production processes. Usually, the biodegradation of these refractory and toxic organic contaminants are often quite slow, and conventional methods may not be very effective (Shang et al., 2021). Furthermore, these traditional treatment methods are often energetically, operationally, or chemically expensive. Therefore, to eliminate these toxic contaminants from wastewater, some alternative and efficient processes must be developed.

With the developing technology, photocatalysis has emerged as a very attractive technology for organic wastewater treatment (Ajmal et al., 2014). During the photocatalytic process, under light irradiation, a series of free radicals can be generated by the catalyst, such as hydroxyl radical ($\cdot OH$), superoxide radical ($\cdot O_2^-$), and holes (h^+). These dissociative radicals can strongly decompose the complex organic contaminants into less toxic products and further transfer them into H_2O and CO_2. Hence, photocatalysts can deal with those organic pollutants harmlessly and efficiently. As the most popular photocatalyst, TiO_2-based nanomaterials are widely regarded as the most dependable photocatalytic materials for decomposing toxic and hazardous organic pollutants (Gaya and Abdullah, 2008). However, in terms of pure TiO_2, because of its large band gap energy (TiO_2, 3.2 eV), it can only absorb a small portion of the solar spectrum in the ultraviolet region (Savio et al., 2016); meanwhile, the rapid recombination of photogenerated e^-/h^+ pairs will reduce the photonic efficiency and decrease its photocatalytic efficiency (Li et al., 2012). Furthermore, the disadvantages of pure TiO_2 particles, such as weak affinity for organic compounds, limited specific surface area, strong agglomeration propensity, and high scattering, which prevents light from reaching active sites on the catalyst surface, restrict their real applicability. As such, significant efforts have been made to modify TiO_2 by doping with nonmetal elements (Patil et al., 2019), noble metals (Alamelu and Jaffar Ali, 2018) or in combination with some narrow band gap semiconductors (Yao et al., 2012), in order to develop highly efficient visible-light-driven photocatalysts. Based on these abovementioned approaches, in our previous report, a nonmetal–metal–semiconductor-promoted photocatalyst (P/$Ag/Ag_2O/Ag_3PO_4/TiO_2$) was successfully developed, which exhibited remarkable photocatalytic ability for decomposing organic matters, water splitting, and bacteria inactivation under simulated solar light irradiation (Liu et al., 2021; Zhu et al., 2021). In addition to improving the photocatalytic efficiency, considering a practical application, the settling of nano-size photocatalysts after the reaction is yet another issue in the liquid medium remediation process due to their small particle size. Therefore, it is necessary to further develop catalysts that are easy to separate and reuse while having high photocatalytic efficiency.

To solve the aforementioned issue, many studies have focused on finding different kinds of supports for dispersing catalysts. These inorganic support materials usually meet the following requirements: 1) significant adsorption affinity toward the organic molecules, 2) exceptional stability in ambient water, and 3) a large specific surface area. Because of these characteristics, organic pollutants degrade much more quickly on their surfaces. Many inorganic support materials have been investigated to help with the photodegradation of environmental pollutants, such as silica (Ren et al., 2009), activated carbon (Li Puma et al., 2008), montmorillonite (Ooka et al., 2003), and zeolite (Huang et al., 2008). These supports act as adsorbents, allowing organic compounds to pre-adsorb and condense on the catalyst surface, thereby promoting photocatalytic activity. Moreover, the support dispersion effect can not only hinder the aggregation of semiconductor particles in the liquid medium but also simplify the separation and reclamation of the photocatalyst from bulk media. Among various adsorbent supports for photocatalysts, zeolite, a porous material with a 3D network structure, was considered the most promising candidate due to its excellent adsorption ability, chemical and thermal stability, abundant reserves, and low cost (Moshoeshoe et al., 2017). In addition, zeolite with a higher affinity to organic pollutants present in the solution helps the reactants get closer proximity to the photocatalysts, which could further enhance the photocatalytic activity (Neppolian et al., 2016). Additionally, zeolite has 4–14 Å cages and channels that can confine substrate molecules to increase the photocatalytic reactivity (Gomez et al., 2013). Therefore, the overall excellent performance of zeolite could accelerate the photocatalytic process by supporting the photocatalyst on zeolite. According to the previous reports, Takashi et al. had researched the enhancement of photocatalytic performance of TiO_2-zeolite

composites for efficient photodegradation of 2-propanol in water (Kamegawa et al., 2013). Zhang et al. prepared a TiO_2/acid leaching zeolite photocatalyst, which displayed superior photocatalytic performance for various organic pollutants removal (Zhang et al., 2018). Alamri et al. developed Fe_2O_3-supported zeolite with the improved elimination of the ofloxacin (Ahmad et al., 2020). Metal oxide (WO_3) and magnetite (Fe_3O_4) based zeolite composite was developed with adsorption enhanced photocatalytic degradation of rhodamine B dye (Rubab et al., 2021). As such, there is an expectation that utilizing zeolite as an adsorbent support could also improve the adsorption capacity of our previously developed P/Ag/Ag_2O/Ag_3PO_4/TiO_2 composite, further improving the photocatalytic activity of the composite. Additionally, in reviewing previous reports, many of the studies have paid great attention to the combination effect of different kinds of adsorbents and photocatalysts while ignoring the effect of the adsorbent ratio presented in the composite. Dependent on the introduction amount of adsorbent, the resulting photocatalysts will show a notable difference in photocatalytic activity (Taoufik et al., 2019). To the best of our understanding on this matter, there is a limited number of research focusing on the information related to the photocatalytic process of zeolite adsorbent–modified photocatalysts with different zeolite additions and their reaction mechanism. As such, it is crucial to find an appropriate zeolite to photocatalyst ratio to synthesize the zeolite-modified P/Ag/Ag_2O/Ag_3PO_4/TiO_2 photocatalyst. To the best of our knowledge, there is no relevant study reported focusing on using zeolite as support for the novel P/Ag/Ag_2O/Ag_3PO_4/TiO_2 photocatalyst for organic wastewater treatment.

Herein, in the present study, the zeolite adsorbent with a 3D network structure was introduced as a carrier to support P/Ag/Ag_2O/Ag_3PO_4/TiO_2 (PAgT) composite for synthesizing the 3D-zeolite–modified photocatalyst (Z-PAgT) *via* a simple hydrothermal method. The physical–chemical structures, morphology, and optical property of Z-PAgT photocatalysts with different zeolite additions were characterized. The photocatalytic activities of the as-prepared photocatalyst were evaluated using photodegradation of rhodamine B (Rh B) under simulated solar light irradiation. Furthermore, the photodegradation mechanism of the novel Z-PAgT photocatalyst was also elucidated.

Materials and methods

Materials

All reagents used in the experiment were of analytical grade and used without further purification. Tetrabutyl titanate [$Ti(OC_4H_9)_4$] (99.5%) as TiO_2 source; silver nitrate ($AgNO_3$) and silver phosphate (Ag_3PO_4) as dopant; ethanol as solvent; HNO_3 as dispersing agent; zeolite (A-3) as adsorbent support; Rh B as model organic pollutant. All the chemicals were purchased from Wako Pure Chemical Industries, Ltd., Japan. All the aqueous solutions were prepared with deionized water.

Synthesis of zeolite-modified photocatalyst

The zeolite-modified photocatalysts (Z-PAgT) were prepared *via* a hydrothermal method. At first, 6 ml tetrabutyl titanate was dissolved in 46 ml ethanol. After stirring for 20 min at ambient temperature, the required amount of $AgNO_3$ (0.1418 g), Ag_3PO_4 (0.1165 g) (same with our previous report (Zhu et al., 2021)), and 11 ml 1 mol/L HNO_3 solution was added dropwise into the compound under vigorous stirring. After stirring for 12 h at room temperature, the homogeneous PAgT sol was obtained. Then, different amounts of zeolite (based on the mass ratio of zeolite/PAgT: 5 wt%, 10 wt%, and 25 wt%) were introduced to the abovestated solution, respectively. Subsequently, the obtained mixture was transferred into a Teflon-lined autoclave. The hydrothermal synthesis was performed at 120 °C for 3 h. Finally, the Z-PAgT photocatalyst powder was obtained after being centrifuged thrice at 9390 × g and dried at 60°C for 12 h. Based on the mass ratio of zeolite/PAgT in photocatalysts, the final products were denoted as Z-PAgT-5, Z-PAgT-10, and Z-PAgT-25, respectively. As a control, the PAgT catalyst without zeolite addition was also prepared under the same condition (donated as Z-PAgT-0).

Characterization of zeolite-modified photocatalyst

X-ray diffraction (XRD) patterns of synthesized photocatalysts were characterized using a Rigaku Altima III Rint-2000 X-ray diffractometer equipped with Cu Kα radiation (λ = 1.54178 Å), and the crystal size was calculated using the Scherrer formula. The functional bonds in the samples were determined *via* Fourier transform-infrared spectrometer (FT-IR, JASCO-6800 spectrophotometer) in the range of 2200–500 cm^{-1}. The morphology and element composition of the prepared photocatalysts were observed using a scanning electron microscopy equipped with energy-dispersive X-ray spectroscopy (SEM, Hitachi FE-SEM S-4800 EDX). The light absorption ability was analyzed using a UV-vis spectrophotometer (UV-vis, JASCO-750V spectrophotometer) in the range of 200–800 nm. Photoluminescence (PL) spectra with an excitation wavelength of 325 nm were recorded in a JASCO FP8500 fluorescence spectrometer. The Brunauer–Emmett–Teller (BET) method was used to determine surface area through Beckman Coulter SA-3100 equipment.

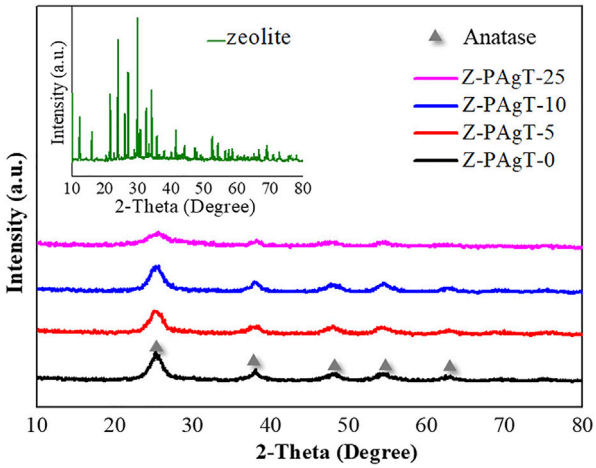

FIGURE 1
XRD patterns of Z-PAgT composite materials with different wt% zeolite addition and pure zeolite (insert).

Evaluation of photocatalytic activity

In this study, the photocatalytic performance of the as-prepared photocatalyst was evaluated through the photodegradation of Rh B in an aqueous solution. The light source during the photocatalytic degradation experiments was provided by a simulated solar lamp (XC-100, SERIC. Ltd., Japan), and the power of this kind of lamp was 100 W. Typically, 0.05 g of the synthesized photocatalyst was dispersed into 50 ml of 2 mg/L Rh B aqueous solution. The mixed solution was first set at a dark condition for 30 min to achieve adsorption–desorption equilibrium under continuous stirring. After 30 min of dark treatment, the solution was irradiated under the simulated solar light (370 nm < λ < 780 nm, 550 W/m^2). Samples were taken out every 15 min, and then the photocatalyst was separated out of the mixture solution by centrifugation. The collected liquid Rh B solution was measured at a wavelength of 554 nm using a spectrophotometer (UV-1500, Shimadzu), which corresponded to the maximum absorption wavelength of Rh B. Meanwhile, a five-cycle experiment was performed to investigate the reusability and stability of the Z-PAgT-5 photocatalyst for practical application. The degradation time for Rh B (50 ml, 2 mg/L) was 60 min per cycle. After each cycle, the photocatalyst was recovered by centrifugation at 9390 × g for 10 min without washing. The recovered photocatalyst was used for subsequent runs under the same reaction conditions as described earlier. To determine the active species, radical trapping experiments were conducted using 1 mM ethylenediamine acetic acid (EDTA) as a hole scavenger, 1-4 benzoquinone (1-4BQ) as a superoxide anion radical scavenger, and tert-butyl alcohol (TBA) as hydroxyl radical scavenger.

Results and discussion

Structure analysis of photocatalysts

The crystal structure and crystallinity of the as-prepared samples were evaluated *via* XRD study. As displayed in Figure 1, the characteristic peaks around 25.3°, 38.0°, 47.8°, 54.3°, and 63.0° which could be attributed to (101), (112), (200), (211), and (204) planes of anatase phase of the TiO_2 can be observed in all prepared photocatalysts. It revealed that no rutile phase was formed in this hydrothermal condition. Usually, the nanocrystalline structure of the anatase phase is more prominent than the rutile phase (Mandal and Bhattacharyya, 2012). In comparison with PAgT alone (Z-PAgT-0), the peaks position of all the zeolite-modified PAgT photocatalysts did not show any obvious change, indicating the introduction of zeolite to PAgT will not destroy the crystal structure or change the crystal phase. However, it was found the intensity of the main anatase TiO_2 peak located at 25.3° showed a sharp decrease with increasing the zeolite wt% to 25. This suggested that the crystallinity of the Z-PAgT-25 sample was relatively worse than the others, which is not conducive to higher photocatalytic performance. Apart from the peaks belonging to TiO_2, the unique zeolite characteristic peaks (as displayed during insert Figure) were not individually appeared in the as-prepared Z-PAgT photocatalyst, which may be mainly due to the low content of zeolite in the hybrid photocatalyst. In addition, no peaks corresponding to the decorated Ag species were detected by the XRD measurement, which could be attributed to the low concentration of Ag species below the XRD detection limit. In addition, the average crystallite size of as-prepared samples was also calculated according to the Debye Scherrer formula and listed in Table 1. Normally, a smaller crystallite size indicates better energy transformation ability, resulting in higher photocatalytic activity (Liu et al., 2020). It can be easily concluded from Table 1 that the order of the crystallite size among all the materials is 25 wt% < 5 wt% < 10 wt % < 0 wt%. The crystallite size was profoundly influenced by different zeolite adding ratios. Although the Z-PAgT-25 sample showed the smallest crystallite size, while comprehensively considering the combined effects of crystallinity (Figure 1) with crystallite size, the Z-PAgT-5 sample may be more favorable to the photocatalytic reaction and possess higher photocatalytic activity.

To identify functional groups presenting on the surface of materials, the FT-IR technique was used, and the transmission spectra of various zeolite-modified PAgT photocatalysts are summarized in Figure 2. The spectra of original zeolite revealed peaks at about 1003 cm^{-1} that can be attributed to antisymmetric stretching of X-O bonds (X = Si or Al) in zeolite-structured aluminosilicates. Around 557 cm^{-1}, a wide band of week intensity was detected, indicating the existence of the zeolite A band assigning the cubic prism. The bands at 468 and 667 cm^{-1} are near the bands at 462 and 668 cm^{-1}, which correspond to the internal linking vibrations of the XO_4 (X = Si or Al) tetrahedra and the asymmetric stretching of zeolite A,

TABLE 1 Structure parameters of Z-PAgT photocatalysts with different zeolite wt%.

Photocatalyst	Crystal size (nm)	Specific surface area (m^2/g)	Band gap (eV)
Z-PAgT-0	4.25	307.19	2.94
Z-PAgT-5	3.96	317.75	2.93
Z-PAgT-10	4.00	320.25	3.00
Z-PAgT-25	3.02	287.62	2.96
Zeolite	—	51.50	—

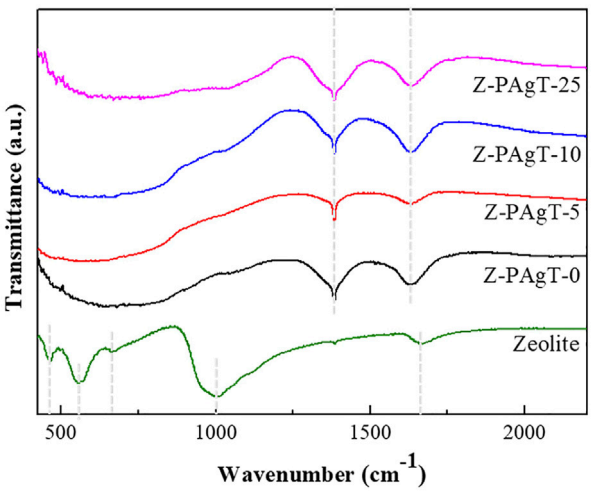

FIGURE 2
FT-IR spectra of the prepared Z-PAgT composite materials with different wt% zeolite addition and pure zeolite.

respectively. The band at 1664 cm^{-1} was attributed to the O-H bond of zeolitic water. As expected, the FT-IR spectrum of each Z-PAgT sample presented a broad band at 1388 cm^{-1}, which was related to the stretching vibrations of the Ti–O bonds in the PAgT photocatalyst. Correspondingly, the distinct peaks observed at 1632 cm^{-1} belongs to Ti-OH functional groups. There is no bond observed at the region of 950–1100 cm^{-1} assigned to the antisymmetric stretching vibration of the Ti-O-Si bond. This result implied that PAgT particles were physically attached to the zeolite surfaces and no chemical bonds were formed at the contact interface between zeolite and PAgT photocatalyst.

Morphology analysis of samples

To investigate the surface morphology and elemental composition of the 3D-zeolite–modified PAgT samples, SEM/EDS analysis was performed. Figure 3 displays the SEM images of zeolite, PAgT, and Z-PAgT with different zeolite wt%. As shown in Figure 3A, the virgin zeolite can be identified by its characteristic cubic morphology with a smooth surface. Followed by a hydrothermal treatment (Figure 3B), the cubic structure subsided slightly compared to the untreated zeolite, which might be attributed to the high temperature and pressure during the hydrothermal process. This subsided zeolite structure could afford more loading sites for the photocatalyst. In the case of the PAgT sample (Z-PAgT-0), as displayed in Figure 3C, its morphology exhibited an irregular shape structure. After introducing zeolite into PAgT photocatalyst (Figures 3D–F), it can be clearly observed that the PAgT composite was successfully distributed on the zeolite surface, and with the increase of zeolite wt%, the number of PAgT particles presenting on the zeolite surface correspondingly decreased. Rougher surface structure was obtained for all hybrid Z-PAgT photocatalysts compared to pure zeolite, which can improve the adsorption capacity of organic molecules and the active sites for the photocatalytic reaction, hence, increasing the photocatalytic activity of the Z-PAgT photocatalyst (Fu et al., 2004). Moreover, in comparison with the PAgT photocatalyst alone, all the particle sizes of Z-PAgT photocatalysts were enlarged, which could inhibit the aggregation of semiconductor particles in a liquid medium and facilitate the post-separation process of the photocatalyst during the practical utilization. The elemental mapping of the Z-PAgT-5 sample revealed the coexistence of Si, Al, Ti, Ag, O, and P elements in the as-prepared sample, confirming the formation of the Z-PAgT photocatalyst (Figure 4). The uniform distribution of these elements in the Z-PAgT-5 sample indicated the PagT photocatalyst was uniformly supported on the zeolite surface. Additionally, the BET surface area (S_{BET}) of Z-PAgT-0, 5, 10, 25 and pure zeolite were determined to be 307.19, 317.75, 320.25, 287.62, and 51.50 m^2/g, respectively (Table 1). The larger specific surface area of the Z-PAgT-5 and 10 photocatalysts suggested that the S_{BET} of the newly developed Z-PAgT photocatalysts can be further enlarged by appropriate zeolite addition, which is beneficial to provide abundant reaction sites and help improve the photocatalytic activity. Based on the abovestated results, it can be concluded that zeolite-modified PAgT materials were successfully fabricated with relatively smaller crystalline size, rougher surface, and larger specific surface area.

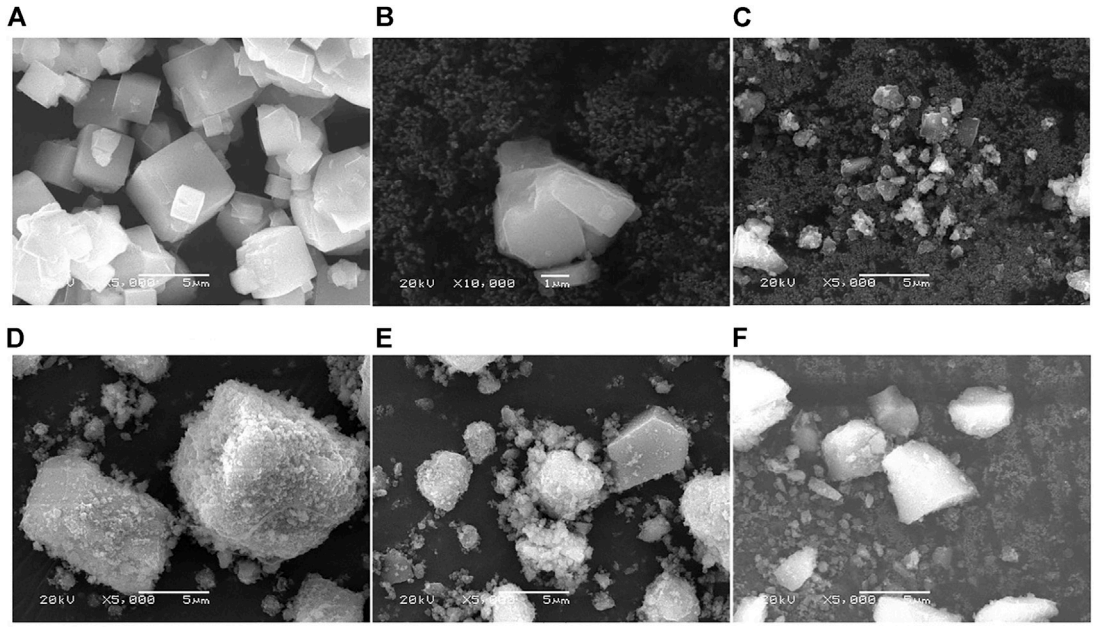

FIGURE 3
SEM images of **(A)** zeolite (original), **(B)** zeolite (by hydrothermal treated), **(C)** Z-PAgT-0, **(D)** Z-PAgT-5, **(E)** Z-PAgT-10, and **(F)** Z-PAgT-25.

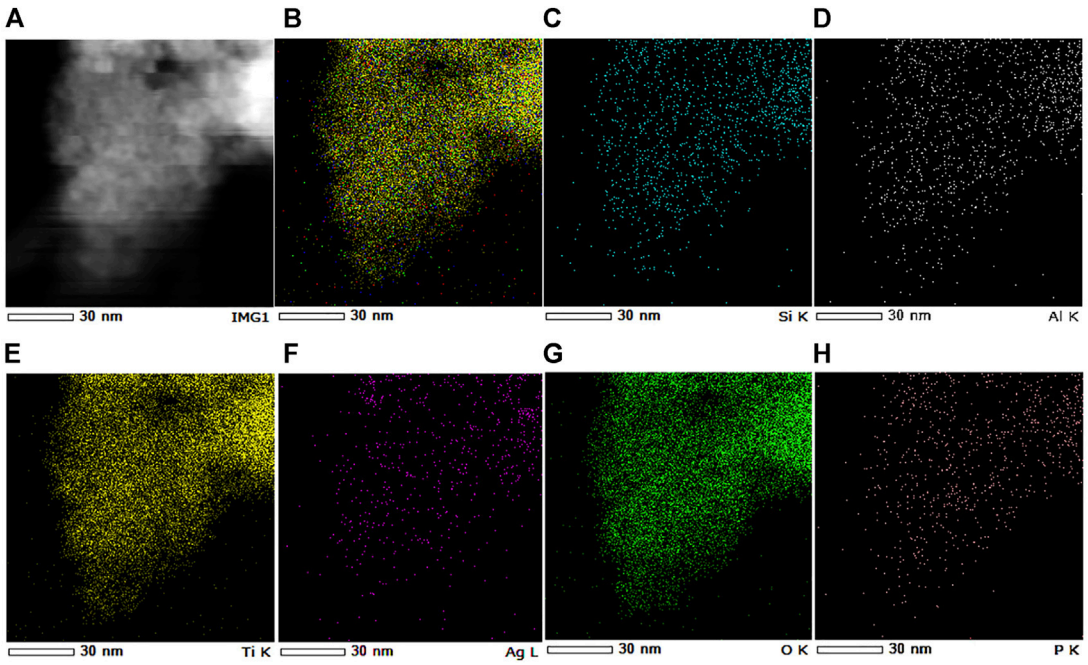

FIGURE 4
Selected area **(A)** and the corresponding EDS elemental mapping of Z-PAgT-5 composite: **(B)** the merged image of all elements, **(C)** Si, **(D)** Al, **(E)** Ti, **(F)** Ag, **(G)** O, and **(H)** P elements.

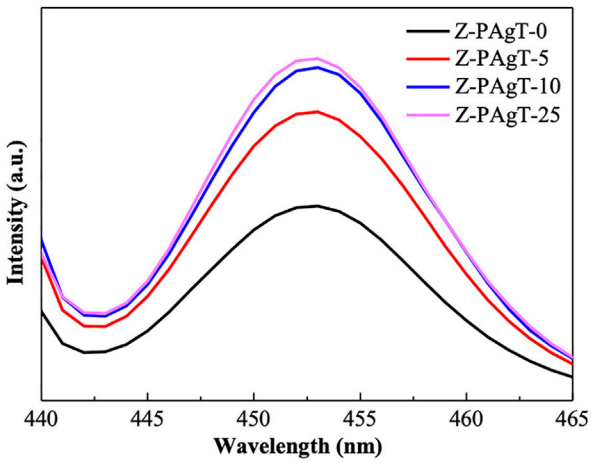

FIGURE 5
PL spectra of the prepared Z-PAgT composite materials with different wt% zeolite addition and pure zeolite.

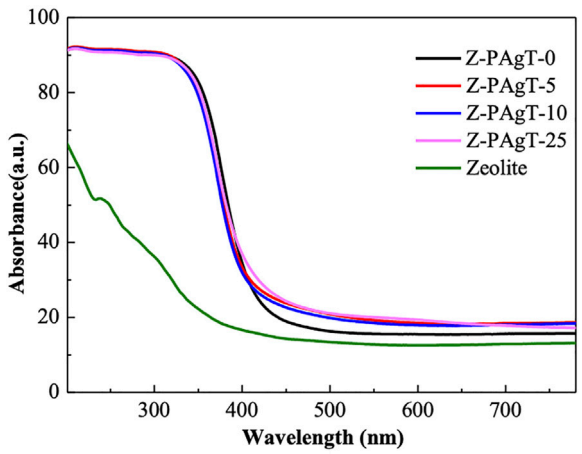

FIGURE 6
UV-vis spectra of the prepared Z-PAgT composite materials with different wt% zeolite addition and pure zeolite.

Optical properties

The photoluminescence (PL) experiment was carried out at room temperature to evaluate the recombination rate of the photo-generated electron and hole pairs (Figure 5). It can be easily concluded from Figure 5 that the sequence of the PL intensities is 0 wt% < 5 wt% < 10 wt% < 25 wt%. The lower PL intensity represents the lower e^-/h^+ pairs recombination rate, which is beneficial for higher photocatalytic activity(Ansari and Cho, 2016). As shown in Figure 5, greater PL intensity was detected on all Z-PAgT photocatalysts when compared to the PL intensity of PAgT (Z-PAgT-0), indicating that the coupling of PAgT with zeolite might boost the recombination of photoelectrons and vacancies. This phenomenon may be mainly attributed to the electron-donating property of zeolite in which the electron-rich sites of the zeolite can donate electrons to photoexcited guests, thereby enhancing the electron-hole pairs recombination rate (Hashimoto, 1997). However, from another point of view, zeolite, as an electron-rich donor, may play a greater role in increasing the concentration of photogenerated electrons per unit volume and lead to an increase in the probability of electrons being captured by oxygen, resulting in more generation of free radicals during the photocatalytic process. In other words, if the separation rate and electron donation rate are faster than the recombination rate of photoelectron and hole pairs, the zeolite-modified PAgT photocatalyst can also obtain higher photocatalytic activity. In addition, among all the Z-PAgT photocatalysts, the Z-PAgT-5 sample exhibited the lowest PL intensity, indicating that it may possess higher photocatalytic activity as compared with other Z-PAgT samples.

UV-vis diffuse reflectance spectroscopy was used to assess the optical absorbance properties of the as-prepared samples. As displayed in Figure 6, it indicated that all the Z-PAgT photocatalysts showed a higher absorption ability in the visible region (400–800 nm) compared with pure zeolite and PAgT sample alone (Z-PAgT-0). This result suggested that after cooperating zeolite with PAgT, the light adsorption ability of the material was enhanced, and the as-prepared zeolite-modified materials could adsorb more light energy during the photodegradation process. To further distinguish the light absorption ability between all samples, the band gap energy was also calculated based on their absorption edge of light (Table 1). It can be figured out that the band gap for Z-PAgT-0, 5, 10 and 25 were 2.94, 2.93, 3.00, and 2.96 eV, respectively. Among them, the Z-PAgT-5 material showed a slightly narrower band gap energy compared to others, which meant that Z-PAgT-5 represented a wider light absorption region. The abovementioned phenomenon may be caused by the uniform distribution of the lower band gap energy of Ag salts on the surface of the zeolite in the as-prepared Z-PAgT-5 material (Gou et al., 2017). In addition, it was reported that the surface roughness and texture of a material can also influence its light absorption capabilities. Hence, the light absorption ability of the Z-PAgT-5 material could have increased because of its rougher surface, as illustrated in the above SEM result (Figure 3) (Roberto Andrade Dantas et al., 2021). The obtained results suggested the Z-PAgT-5 catalyst with improved light absorption may have increased photonic activation for effective pollutant removal in wastewater.

Photocatalytic activity

After a series of material characterizations, the photocatalytic degradation efficiency of the prepared photocatalysts was further

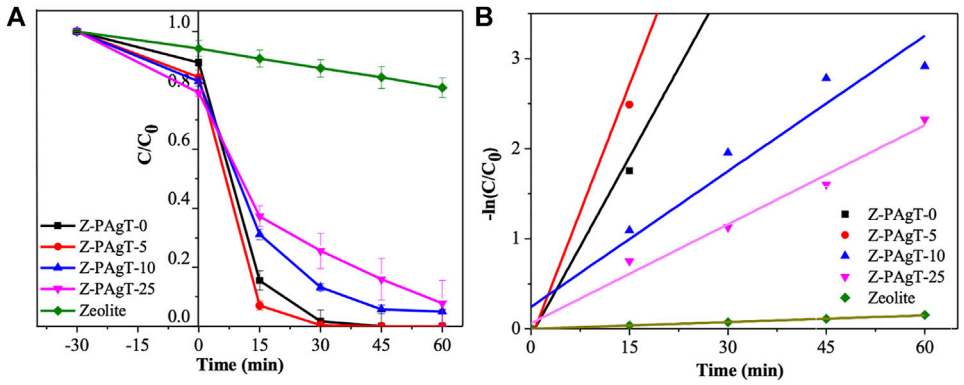

FIGURE 7
(A) Degradation rate and **(B)** first-order kinetic result of Rh B by zeolite modified PAgT composites with different wt% zeolite addition under simulated solar light irradiation.

examined by the oxidation of Rh B, a typical organic pollutant in wastewater. As seen in Figure 7A, during the first 30 min of dark treatment, the adsorption reaction occurred within all the samples. Among these samples, Z-PAgT samples with different wt% of zeolite have an outstanding adsorption capacity compared with PAgT (Z-PAgT-0) and pure zeolite. In addition, the adsorption efficiency of Z-PAgT material was found to increase with the increase of zeolite wt%. This is due to the strong adsorption and affinity ability of the zeolite on Rh B molecules. This property is conducive to bringing Rh B closer to the photocatalyst surface and improving the subsequent photocatalytic degradation. After starting the irradiation by simulated solar light, it is evident that the Z-PAgT-5 photocatalyst holds the optimal performance among the five samples, and, within only 30 min of irradiation, a complete removal efficiency of Rh B can be achieved. The photocatalytic degradation kinetics for Rh B degradation of all the samples is illustrated in Figure 7B, which can be expressed by a pseudo-first-order reaction equation. The calculated reaction rate constant (k_{app}) from all samples is shown in Supplementary Table S1. It is evident that Z-PAgT-5 possessed the highest k_{app} (0.188 min^{-1}) for Rh B degradation as compared to that of Z-PAgT-0 (0.132 min^{-1}), Z-PAgT-10 (0.050 min^{-1}), Z-PAgT-25 (0.037 min^{-1}), and pure zeolite (0.003 min^{-1}), which indicated that adding the appropriate zeolite could further enhance the photocatalytic activity of PAgT photocatalyst. In summary, the results verified the advantages of adsorption and photodegradation synergism between zeolite and PAgT, indicating that combining PAgT with appropriate zeolite addition could further enhance the photocatalytic activity due to the positive synergetic effect of the adsorption and photodegradation process. In this study, 5 wt% zeolite was found to be the optimal addition for the preparation of hybrid Z-PAgT photocatalysts. The strong adsorption and outstanding photocatalytic degradation of Rh B verified that Z-PAgT-5 is a good candidate for photocatalytic oxidation of organic pollutants in wastewater.

Stability of the prepared 3D-zeolite–modified photocatalyst

The stability of the photocatalyst was an important parameter during the practical application for the removal of pollutants. Therefore, to evaluate the stability and practicability of the developed 3D-zeolite–modified photocatalyst material, consecutive photodegradation experiments were performed by using Z-PAgT-5 as the catalyst. As shown in Figure 8A, Z-PAgT-5 possessed a good stable photodegradation efficiency. Even after five cycles of photocatalytic reaction, the Z-PAgT-5 material still exhibited strongly photodegradation ability. This indicated that Z-PAgT-5 photodegradation carried out under ambient conditions without the use of harsh regenerative procedures such as ultrasonication, washing, and drying demonstrated good stability and reusability. During the first three circles, the photocatalytic performance was hardly reduced. Only a slight decrease was observed after the third cycle, which may be due to the blocking of the material pores by Rh B molecules during the adsorption process and the loss of the photocatalyst during the collection process. Moreover, the stability of the Z-PAgT-5 photocatalyst was further confirmed by XRD analysis before and after five photocatalytic reactions. As seen in Figure 8B, the characteristic peaks and crystal phase observed from the XRD patterns showed no change in the photocatalyst even after five cycles, indicating good stability of the Z-PAgT-5 material during the catalytic reaction. Additionally, in order to further investigate the photocatalytic ability of Z-PAgT-5, the photocatalytic efficiency (amount of pollutants that can be

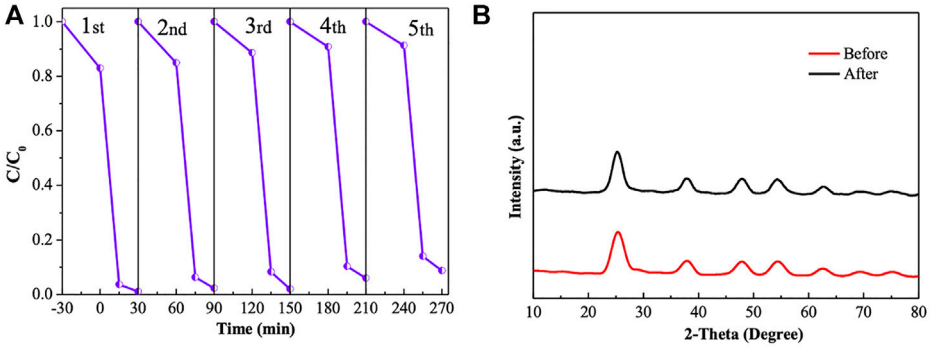

FIGURE 8
(A) Recycling experiment of Z-PAgT-5 material for Rh B degradation (dark 30 min and light 30 min) and **(B)** XRD patterns of Z-PAgT-5 material before and after five recycles.

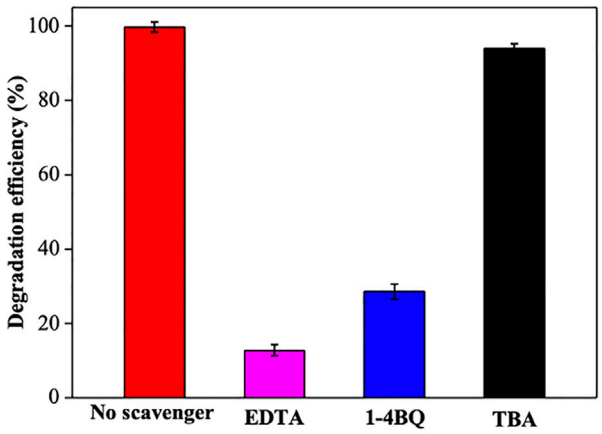

FIGURE 9
Scavenger study during Z-PAgT-5 photocatalytic degradation reaction under simulated solar light (dark 30 min and light 30 min).

degraded by unit mass of photocatalyst per minute) was also calculated and compared with other reported photocatalysts. As shown in Supplementary Table S2, it was found that among all materials, Z-PAgT-5 displayed the highest degradation efficiency with 0.067 mg/g/min, indicating its high photocatalytic removal ability for Rh B. As for Zeolite/g-C_3N_4 (Kumar et al., 2018), CdS/TiO_2 (Wang et al., 2019), SiO_2/CNOs/TiO_2 (3%) (Zhang et al., 2019), g-C_3N_4/Ag–TiO_2 (2%) (Sui et al., 2020), and Nb-doped TiO_2/rGO (Prabhakarrao et al., 2021), their photocatalytic efficiency was dramatically lower than Z-PAgT-5. As such, all the abovestated results suggest that our created Z-PAgT-5 photocatalyst with high photocatalytic efficiency and stability for numerous cycles is a promising alternative for wastewater treatment in practical applications.

Proposed mechanism

To identify the dominant active species involved during the Z-PAgT photocatalytic degradation process, radical trapping experiments were conducted. In this study, EDTA, 1-4BQ, and TBA were introduced as scavengers of holes (h^+), superoxide anion ($\bullet O_2^-$), and hydroxyl radical (•OH), respectively. As seen in Figure 9, compared with the photocatalytic reaction without scavenger, the addition of EDTA and 1-4BQ significantly inhibited the degradation efficiency of Rh B, proving that h^+ and $\bullet O_2^-$ played an important role in the degradation process. However, when TBA was added to the solution, only a slight decrease in the degradation efficiency was observed as compared with that of no scavenger added, implying that •OH had a minor effect on the photocatalytic process. In brief, the abovestated results indicate that h^+ and $\bullet O_2^-$ are the major reactive species contributing to the enhanced degradation process in the present Z-PAgT photocatalytic system.

By combining our previous characterization data with photodegradation results on zeolite-modified PAgT photocatalysts, a possible mechanism for the photocatalytic elimination of Rh B by Z-PAgT-5 under simulated solar light irradiation in an aqueous solution was proposed (Figure 10). During the synthesis process, when the zeolite was introduced into the prepared PAgT sol, after hydrothermal treatment, the catalyst PAgT particles could be uniformly distributed on the surface of the zeolite. Before photocatalysis, the adsorption of the photocatalyst served as a key process in removing the dissolved organic pollutant. Due to the superior affinity and adsorption capability of zeolite toward organic substances, hence, the zeolite-supported PAgT photocatalyst can adsorb or condense an enormous number of organic molecules from water on its surfaces. Moreover, the adsorbed Rh B molecules can migrate to the catalyst's internal and exterior active sites, allowing more contaminants to react with the supported photocatalyst. Then, after turning on the solar light illumination, the photocatalytic

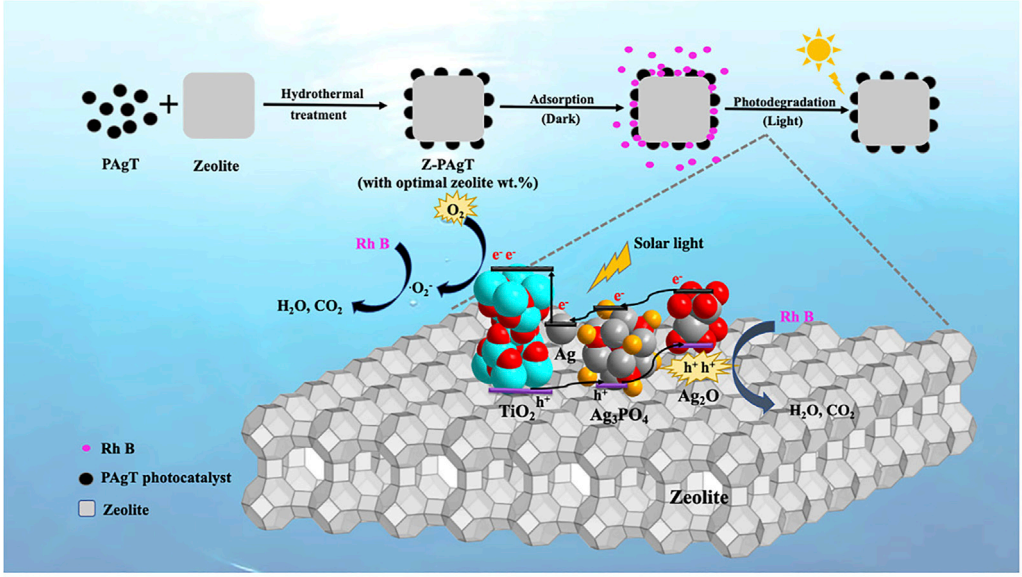

FIGURE 10
Proposed mechanism of Z-PAgT-5 composite for Rh B degradation under simulated solar light.

process will be involved to be responsible for the Rh B degradation. In detail, the Z-PAgT-5 photocatalyst can be photoexcited to generate e^- and h^+. The e^- would be efficiently trapped at less negative Ag because the conduction band potentials of Ag_3PO_4 (0.45 eV vs. NHE) and Ag_2O (0.2 eV vs. NHE) are more negative than the Fermi level of the Ag nanoparticles (0.99 eV vs. NHE), which would then be transported to the surface of TiO_2 through the surface plasmon resonance effect (SPR) and combine with surface O_2 to produce superoxide radicals ($\bullet O_2^-$). Accordingly, the produced h^+ moves to more positive Ag_2O because the valence band of TiO_2 (2.91 eV vs. NHE) and Ag_3PO_4 (2.88 eV vs. NHE) are more positive than that of Ag_2O (1.4 eV vs. NHE), which can oxidize organic contaminants in the solution directly. Meanwhile, hydroxyl radicals ($\bullet OH$) can be formed when photogenerated h^+ oxidizes adsorbed H_2O. All of these photogenerated radicals can react with the pre-adsorbed organic Rh B molecules and, finally, transfer them to CO_2 and H_2O. The enhancement of photocatalytic performance over the Z-PAgT-5 sample is related closely to the coupling effect between the zeolite support and PAgT catalyst. The abovestated photodegradation results (Figure 7) showed that depending on the introduction amount of zeolite, the resulting zeolite contained PAgT samples showed a notable difference in photocatalytic activity. This is because the added amount of Z-PAgT photocatalyst is constant across all photocatalytic degradation studies (0.05 g). Hence, as the zeolite concentration increases from 0% to 25%, the PAgT amount in the photocatalyst decreases from 100% to 75%. In other words, the incorporation of zeolite into produced photocatalysts can boost adsorption while decreasing photocatalytic activity. Consequently, the degrading activity of photocatalysts appears to be at its peak when the zeolite mass ratio is 5 wt%. This is the synergetic effect between zeolite adsorbent support and PAgT photocatalyst, making the Z-PAgT-5 photocatalyst possess good adsorption and photodegradation properties. In addition, the larger particle size of zeolite helps to increase the dispersion of PAgT particles onto the zeolite support, which can efficiently reduce the particle aggregation, facilitate the post-separation process, and enhance the reusability of the Z-PAgT-5 photocatalyst. Therefore, it is expected that Z-PAgT-5 can be a promising candidate in view of future practical applications in environmental remediation.

Conclusion

In this study, 3D-zeolite–modified PAgT photocatalysts were successfully synthesized *via* a hydrothermal method by using PAgT as photocatalyst and zeolite as adsorbent support. The characterization results of the prepared photocatalysts showed that PAgT particles were covered onto the surface of zeolite to form the hybrid Z-PAgT photocatalysts, which indicated the close combination of PAgT and zeolite support. It is very important to choose appropriate zeolite addition (wt%) to obtain the optimal adsorption capacity and photodegradation activity of the prepared materials. Results revealed the Z-PAgT photocatalyst modified with an optimum mass ratio of zeolite addition (5 wt%) exhibited relatively better crystallinity, smaller

crystalline size, narrower band gap, larger specific surface area, and lower generated electron-hole pairs recombination rate. As expected, the Z-PAgT-5 photocatalyst exhibited rapid photocatalytic performance for the decomposition of Rh B under simulated solar light irradiation. This phenomenon could be attributed to the positive synergetic effect between zeolite adsorbent support and PAgT photocatalyst, making the Z-PAgT-5 photocatalyst possess good adsorption and photodegradation properties. Furthermore, the Z-PAgT-5 photocatalyst displayed high stability even after consecutive utilization for five times, which indicates that it can be promisingly applied in practical wastewater purification.

Data availability statement

The original contributions presented in the study are included in the article/Supplementary Material, further inquiries can be directed to the corresponding author.

Author contributions

NL: conceptualization, formal analysis, investigation, methodology, visualization, writing—original draft preparation, writing—review and editing, and funding acquisition. RQ: investigation, methodology, and writing—review and editing. XS: methodology and writing—review. NK: methodology and resources. GC: methodology and writing—review and editing. YY: conceptualization, funding acquisition, investigation, methodology, project administration, data curation, supervision, and writing—review and editing.

Funding

This work was kindly funded by Grant-in-Aid for Exploratory Research 21k19628 from the Japan Society for the Promotion of Science, the Science and Technology Project of Hebei Education Department (BJK2022035), and High-level Talents Research Start-up Fund-Nature of Chengde Medical University (202205).

Conflict of interest

The authors declare that the research was conducted in the absence of any commercial or financial relationships that could be construed as a potential conflict of interest.

Publisher's note

All claims expressed in this article are solely those of the authors and do not necessarily represent those of their affiliated organizations, or those of the publisher, the editors, and the reviewers. Any product that may be evaluated in this article, or claim that may be made by its manufacturer, is not guaranteed or endorsed by the publisher.

Supplementary material

The Supplementary Material for this article can be found online at: https://www.frontiersin.org/articles/10.3389/fenvs.2022.1009045/full#supplementary-material

References

Ahmad, A. R. D., Imam, S. S., Oh, W. D., and Adnan, R. (2020). Fe3O4-zeolite hybrid material as hetero-fenton catalyst for enhanced degradation of aqueous ofloxacin solution. *Catalysts* 10 (11), 1241–1319. doi:10.3390/catal10111241

Ajmal, A., Majeed, I., Malik, R. N., Idriss, H., and Nadeem, M. A. (2014). Principles and mechanisms of photocatalytic dye degradation on TiO 2 based photocatalysts: a comparative overview. *RSC Adv.* 4 (70), 37003–37026. doi:10.1039/c4ra06658h

Alamelu, K., and Jaffar Ali, B. M. (2018). TiO2-Pt composite photocatalyst for photodegradation and chemical reduction of recalcitrant organic pollutants. *J. Environ. Chem. Eng.* 6 (5), 5720–5731. doi:10.1016/j.jece.2018.08.042

Ansari, S. A., and Cho, M. H. (2016). Highly visible light responsive, narrow band gap TiO2 nanoparticles modified by elemental red phosphorus for photocatalysis and photoelectrochemical applications. *Sci. Rep.* 6, 25405–25410. Nature Publishing Group. doi:10.1038/srep25405

Fu, P., Luan, Y., and Dai, X. (2004). Preparation of activated carbon fibers supported TiO2 photocatalyst and evaluation of its photocatalytic reactivity. *J. Mol. Catal. A Chem.* 221 (1–2), 81–88. doi:10.1016/j.molcata.2004.06.018

Gaya, U. I., and Abdullah, A. H. (2008). Heterogeneous photocatalytic degradation of organic contaminants over titanium dioxide: A review of fundamentals, progress and problems. *J. Photochem. Photobiol. C Photochem. Rev.* 9 (1), 1–12. doi:10.1016/j.jphotochemrev.2007.12.003

Gomez, S., Marchena, C. L., Pizzio, L., and Pierella, L. (2013). Preparation and characterization of TiO2/HZSM-11 zeolite for photodegradation of dichlorvos in aqueous solution. *J. Hazard. Mater.* 258–259, 19–26. Elsevier B.V. doi:10.1016/j.jhazmat.2013.04.030

Gou, J., Ma, Q., Deng, X., Cui, Y., Zhang, H., Cheng, X., et al. (2017). Fabrication of Ag2O/TiO2-Zeolite composite and its enhanced solar light photocatalytic performance and mechanism for degradation of norfloxacin. *Chem. Eng. J.* 308, 818–826. Elsevier B.V. doi:10.1016/j.cej.2016.09.089

Hashimoto, S. (1997). Zeolites as single electron donors for photoinduced electron transfer reactions of guest aromatic species diffuse reflectance laser photolysis study. *Faraday Trans.* 93 (24), 4401–4408. doi:10.1039/a704955b

Huang, M., Xu, C., Wu, Z., Huang, Y., Lin, J., and Wu, J. (2008). Photocatalytic discolorization of methyl orange solution by Pt modified TiO2 loaded on natural zeolite. *Dyes Pigm.* 77 (2), 327–334. doi:10.1016/j.dyepig.2007.01.026

Kamegawa, T., Kido, R., Yamahana, D., and Yamashita, H. (2013). Design of TiO 2-zeolite composites with enhanced photocatalytic performances under irradiation of UV and visible light. *Microporous Mesoporous Mater.* 165, 142–147. Elsevier Inc. doi:10.1016/j.micromeso.2012.08.013

Kumar, A., Samanta, S., and Srivastava, R. (2018). Systematic investigation for the photocatalytic applications of carbon nitride/porous zeolite heterojunction. *ACS Omega* 3 (12), 17261–17275. doi:10.1021/acsomega.8b01545

Li, Y., Zhou, X., Chen, W., Li, L., Zen, M., Qin, S., et al. (2012). Photodecolorization of Rhodamine B on tungsten-doped TiO 2/activated carbon under visible-light irradiation. *J. Hazard. Mater.* 227–228, 25–33. Elsevier B.V. doi:10.1016/j.jhazmat.2012.04.071

Li Puma, G., Bono, A., Krishnaiah, D., and Collin, J. G. (2008). Preparation of titanium dioxide photocatalyst loaded onto activated carbon support using chemical vapor deposition: A review paper. *J. Hazard. Mater.* 157 (2–3), 209–219. doi:10.1016/j.jhazmat.2008.01.040

Liu, X., Zhu, L., Wang, X., and Meng, X. (2020). Photocatalytic degradation of wastewater by molecularly imprinted Ag2S-TiO2 with high-selectively. *Sci. Rep.* 10 (1), 1192–1210. doi:10.1038/s41598-020-57925-8

Liu, N., Ming, J., Sharma, A., Sun, X., Kawazoe, N., Chen, G., et al. (2021). Sustainable photocatalytic disinfection of four representative pathogenic bacteria isolated from real water environment by immobilized TiO2-based composite and its mechanism. *Chem. Eng. J.* 426, 131217. Elsevier B.V. doi:10.1016/j.cej.2021.131217

Mandal, S. S., and Bhattacharyya, A. J. (2012). Electrochemical sensing and photocatalysis using Ag-TiO 2 microwires. *J. Chem. Sci.* 124, 969–978. doi:10.1007/s12039-012-0290-9

Moshoeshoe, M., Silas Nadiye-Tabbiruka, M., and Obuseng, V. (2017). A review of the chemistry, structure, properties and applications of zeolites. *Am. J. Mater. Sci.* 2017 (5), 196–221. doi:10.5923/j.materials.20170705.12

Neppolian, B., Mine, S., Horiuchi, Y., Bianchi, C., Matsuoka, M., Dionysiou, D., et al. (2016). Efficient photocatalytic degradation of organics present in gas and liquid phases using Pt-TiO2/Zeolite (H-ZSM). *Chemosphere* 153, 237–243. doi:10.1016/j.chemosphere.2016.03.063

Ooka, C., Yoshida, H., Horio, M., Suzuki, K., and Hattori, T. (2003). Adsorptive and photocatalytic performance of TiO2 pillared montmorillonite in degradation of endocrine disruptors having different hydrophobicity. *Appl. Catal. B Environ.* 41 (3), 313–321. doi:10.1016/S0926-3373(02)00169-8

Patil, S. B., Basavarajappa, P. S., Ganganagappa, N., Jyothi, M., Raghu, A., and Reddy, K. R. (2019). Recent advances in non-metals-doped TiO2 nanostructured photocatalysts for visible-light driven hydrogen production, CO2 reduction and air purification. *Int. J. Hydrogen Energy* 44 (26), 13022–13039. Elsevier Ltd. doi:10.1016/j.ijhydene.2019.03.164

Prabhakarrao, N., Rao, T. S., Lakshmi, K. V. D., Divya, G., Jaishree, G., Raju, I. M., et al. (2021). Enhanced photocatalytic performance of Nb doped TiO2/reduced graphene oxide nanocomposites over rhodamine B dye under visible light illumination. *Sustain. Environ. Res.* 31 (1), 37–21. doi:10.1186/s42834-021-00110-x

Ren, S., Zhao, X., Zhao, L., Yuan, M., Yu, Y., Guo, Y., et al. (2009). Preparation of porous TiO2/silica composites without any surfactants. *J. Solid State Chem.* 182 (2), 312–316. doi:10.1016/j.jssc.2008.10.027

Roberto Andrade Dantas, S., de Oliveira Romano, R. C., Vittorino, F., and Loh, K. (2021). Effects of surface roughness and light scattering on the activation of TiO2 on mortar photocatalytic process. *Constr. Build. Mater.* 270, 121421. doi:10.1016/j.conbuildmat.2020.121421

Rubab, M., Bhatti, I. A., Nadeem, N., Shah, S. A. R., Yaseen, M., Naz, M. Y., et al. (2021). Synthesis and photocatalytic degradation of rhodamine B using ternary zeolite/WO $_3$/Fe $_3$ O $_4$ composite. *Nanotechnology* 32 (34), 345705. doi:10.1088/1361-6528/ac037f

Savio, A. K. P. D., Fletcher, J., Smith, K., Iyer, R., Bao, J., and Robles Hernandez, F. (2016). Environmentally effective photocatalyst CoO-TiO2 synthesized by thermal precipitation of Co in amorphous TiO2. *Appl. Catal. B Environ.* 182, 449–455. doi:10.1016/j.apcatb.2015.09.047

Shang, J., Jiang, Y., Qin, X., Zhao, B., and Li, X. (2021). Catalytic oxidation of methylene blue by attapulgite/TiO2. *Front. Environ. Sci.* 9, 1–9. doi:10.3389/fenvs.2021.783313

Sui, G., Li, J., Du, L., Zhuang, Y., Zhang, Y., Zou, Y., et al. (2020). Preparation and characterization of g-C3N4/Ag–TiO2 ternary hollowsphere nanoheterojunction catalyst with high visible light photocatalytic performance. *J. Alloys Compd.* 823, 153851. Elsevier B.V. doi:10.1016/j.jallcom.2020.153851

Takala, A. (2017). Understanding sustainable development in Finnish water supply and sanitation services. *Int. J. Sustain. Built Environ.* 6 (2), 501–512. The Gulf Organisation for Research and Development. doi:10.1016/j.ijsbe.2017.10.002

Taoufik, N., Elmchaouri, A., Anouar, F., Korili, S. A., and Gil, A. (2019). Improvement of the adsorption properties of an activated carbon coated by titanium dioxide for the removal of emerging contaminants. *J. Water Process Eng.* 31, 100876. Elsevier. doi:10.1016/j.jwpe.2019.100876

Wang, H., Li, J., Zhou, H., Yao, S., and Zhang, W. (2019). Template synthesis and characterization of CdS/TiO2 coaxial nanocables for photocatalysis in visible light. *J. Mater. Sci. Mater. Electron.* 30 (11), 10754–10764. Springer US. doi:10.1007/s10854-019-01419-5

Yao, W., Zhang, B., Huang, C., Ma, C., Song, X., and Xu, Q. (2012). Synthesis and characterization of high efficiency and stable Ag 3PO 4/TiO 2 visible light photocatalyst for the degradation of methylene blue and rhodamine B solutions. *J. Mater. Chem.* 22 (9), 4050–4055. doi:10.1039/c2jm14410g

Zhang, G., Song, A., Duan, Y., and Zheng, S. (2018). Enhanced photocatalytic activity of TiO2/zeolite composite for abatement of pollutants. *Microporous Mesoporous Mater.* 255, 61–68. Elsevier Ltd. doi:10.1016/j.micromeso.2017.07.028

Zhang, W., Zhang, Y., Yang, K., Yang, Y., Jia, J., and Guo, L. (2019). Photocatalytic performance of SiO2/CNOs/TiO2 to accelerate the degradation of rhodamine B under visible light. *Nanomaterials* 9 (12), 1671. doi:10.3390/nano9121671

Zhu, Q., Liu, N., Ma, Q., Sharma, A., Nagai, D., Sun, X., et al. (2021). Sol-gel/hydrothermal two-step synthesis strategy for promoting Ag species–modified TiO2-based composite activity toward H2 evolution under solar light. *Mater. Today Energy* 20, 100648. Elsevier Ltd. doi:10.1016/j.mtener.2021.100648